2176–2193 *Nucleic Acids Research, 2009, Vol. 37, No. 7* *Published online 19 February 2009*
doi:10.1093/nar/gkp082

RAD18 promotes DNA double-strand break repair during G1 phase through chromatin retention of 53BP1

Kenji Watanabe[1], Kuniyoshi Iwabuchi[2], Jinghua Sun[1], Yuri Tsuji[1,3], Tokio Tani[4], Kazuaki Tokunaga[4], Takayasu Date[2], Mitsumasa Hashimoto[2], Masaru Yamaizumi[1,†] and Satoshi Tateishi[1,*]

[1]Cell Genetics, Institute of Molecular Embryology and Genetics, Kumamoto University, Kumamoto 860-0811, [2]Department of Biochemistry, Kanazawa Medical University, Daigaku 1-1, Uchinada, Kahoku-gun, Ishikawa 920-0293, [3]Department of Oral and Maxillofacial Surgery, Sensory and Motor Organs Sciences, Faculty of Medicine and Pharmaceutical Sciences, Kumamoto University, Kumamoto 860-0811 and [4]Department of Biological Science, Faculty of Science, Kumamoto University, Kumamoto 860-8555, Japan

Received September 17, 2008; Revised January 14, 2009; Accepted January 28, 2009

ABSTRACT

Recruitment of RAD18 to stalled replication forks facilitates monoubiquitination of PCNA during S-phase, promoting translesion synthesis at sites of UV irradiation-induced DNA damage. In this study, we show that RAD18 is also recruited to ionizing radiation (IR)-induced sites of DNA double-strand breaks (DSBs) forming foci which are co-localized with 53BP1, NBS1, phosphorylated ATM, BRCA1 and γ-H2AX. RAD18 associates with 53BP1 and is recruited to DSB sites in a 53BP1-dependent manner specifically during G1-phase, RAD18 monoubiquitinates KBD domain of 53BP1 at lysine 1268 *in vitro*. A monoubiquitination-resistant 53BP1 mutant harboring a substitution at lysine 1268 is not retained efficiently at the chromatin in the vicinity of DSBs. In *Rad18*-null cells, retention of 53BP1 foci, efficiency of DSB repair and post-irradiation viability are impaired compared with wild-type cells. Taken together, these results suggest that RAD18 promotes 53BP1-directed DSB repair by enhancing retention of 53BP1, possibly through an interaction between RAD18 and 53BP1 and the modification of 53BP1.

INTRODUCTION

Genetic screening of *Saccharomyces cerevisiae* mutants has shown that *RAD18*, a RING-type (E3) ubiquitin ligase, is involved in the post-replication repair pathway (1). Yeast *RAD18* mutants are hypersensitive to various DNA-damaging agents, including UV light, γ rays and certain chemicals (2). Mammalian RAD18 also plays a crucial role in post-replication repair. In human cells, only one homolog of *RAD18* has been identified (3). *Rad18*-knockout mouse embryonic stem cells and chicken DT40 cells are sensitive to various DNA-damaging agents and display enhanced genomic instability (4,5). Similar to its yeast homolog, human RAD18 forms a complex with RAD6 (an E2 ubiquitin-conjugating enzyme) and monoubiquitinates proliferating cell nuclear antigen (PCNA) at replication forks that are stalled by UV-induced (and other) DNA lesions (6,7).

We previously demonstrated that RAD18 rapidly translocates to the nuclei of UV-irradiated mammalian cells, accumulating at sites of stalled replication as discrete observable foci. Fluorescence microscopy has shown that these foci colocalize with DNA polymerase η (Polη) and PCNA. We found that human RAD18 also translocates to the nucleus in response to replication stress induced by dNTP depletion or the acquisition of double-strand DNA breaks (DSBs) (8). When stalled replication forks cannot be resolved and collapse to

*To whom correspondence should be addressed. Tel: +81 96 373 6602; Fax: +81 96 373 6604; Email: tate@gpo.kumamoto-u.ac.jp
†Dr M. Yamaizumi died in May 2006.

The authors wish it to be known that, in their opinion, the first two authors should be regarded as joint First Authors.

generate DSBs, vertebrate RAD18 facilitates homologous recombination at the sites of breakage, reducing the cytotoxic effect of DSB-inducing agents (9).

Recently, it was demonstrated that *RAD18*-null HCT116 cells are sensitive to both X-ray irradiation and camptothecin, due to the defective repair of single-strand DNA breaks that arise during S-phase (10). These observations indicate that mammalian RAD18 responds to a numerous forms of DNA damage in addition to that induced by UV irradiation. In X-irradiated cells, Polη focus formation and PCNA monoubiquitination have not been observed (10,11). In contrast with Polη and ubiquitinated PCNA, which are unresponsive to DSBs, RAD18 is rapidly dispersed throughout the nucleus following X-ray irradiation, and it exhibits dynamic behavior similar to that observed in UV-irradiated cells. These findings suggest that RAD18 is involved in the cellular response to DSBs via PCNA- and Polη-independent mechanisms. However, the sensitivity of *Rad18*-null mouse embryonic stem cells and fibroblasts to IR is not significantly higher than that of wild-type (wt) cells (4,12); thus, the putative role of RAD18 in the response to DSBs is unclear.

Therefore, in the present study, we investigated the regulation and function of RAD18 in response to DSBs. In cells exposed to DSB-inducing agents, many proteins involved in the DNA damage-response pathway, including BRCA1, MRE11/NBS1/RAD50 and 53BP1, accumulate in nuclear foci. These foci have been designated IR-induced nuclear foci (IRIFs) (13,14). γ-H2AX, which is immediately phosphorylated at its C-terminus in response to DSBs, plays a crucial role in regulating IRIF formation. Many components of IRIFs colocalize with γ-H2AX foci, and γ-H2AX is required for the retention of NBS1 and 53BP1 at DSBs (15). IRIF formation is thought to be vital for cellular DNA repair and the activation of DNA-damage checkpoints (16). The function of RAD18 in IR-irradiated cells and the potential targets of its E3 ligase activity are unknown. Therefore, in the present study we sought to identify the role of RAD18 in the DSB response, and to determine the relationship between IRIFs and RAD18 foci. The results presented here identify 53BP1 as a novel substrate of RAD18-directed E3 ligase activity and demonstrate the key role of mammalian RAD18 in maintaining 53BP1 IRIFs. Importantly, we show that *Rad18*-null mouse embryonic fibroblasts (MEFs) exhibit defects in DSB repair. Taken together, these results suggest that RAD18 plays a critical role in the DSB damage-response pathway.

MATERIALS AND METHODS

Antibodies (Abs)

Abs specific for Ser139-phosphorylated histone H2A.X and Ser10-phosphorylated Histone H3 were purchased from Upstate. Abs specific for ATMpS1981 and BRCA1 (Ab-1) were purchased from Rockland and Oncogene, respectively. Monoclonal anti-FLAG (M5) Abs were purchased from Sigma, while monoclonal anti-nibrin (C-19), −HA and c-Myc Abs were purchased from Santa Cruz Biotechnology. Monoclonal Abs against 53BP1 (BP13 and BP18) were purchased from Upstate, whereas polyclonal Abs against 53BP1 (Ab-1) were obtained from Oncogene. The rabbit polyclonal Abs against human and mouse RAD18 are described elsewhere (4,6).

Cell lines

Rad18-null and wt mouse fibloblasts have been described elsewhere (6). To obtain stable transformants of *Rad18*-null cells expressing wt Rad18, or zinc-finger or RAD6-binding domain deletion derivatives of Rad18, *Rad18*-null cells were cotransfected with pcDNA3.1/Hygro (Invitrogen) and vectors containing wt or mutant pCAGGS-*Rad18*. Cells were selected with hygromycin B (50 μg/ml), and surviving colonies were cloned. Expression of transgenes was confirmed by immunofluorescence staining and western blotting using anti-mouse Rad18 Abs. Mouse embryonic fibroblasts (MEFs) were isolated from mouse embryos taken from C57BL6/J mothers at 13.5 days of gestation. 53BP1-null MEFs were kindly provided by Dr J.Chen. DNA-PK Inhibitor II (NU7026) and bleomycin were purchased from Calbiochem.

Cell synchronization and X-ray survival assay

For synchronization of HeLa cells, the double thymidine block method was used. In brief, after thymidine was added at a concentration of 1 mM, cells were cultured for 24 h, and then cultured for 8 h in normal medium. After a second addition of thymidine at 1 mM, cells were cultured for 14 h. These cells were then cultured again in normal medium, thereby releasing them from cell cycle arrest at G_1/S. FACS analysis was used to verify the cell synchronization. HeLa cells enriched in G1, S and G2/M phase populations were X-irradiated with 5 Gy and incubated for 1 h prior to analysis by immunofluorescence microscopy. To enrich for quiescent (G0) populations, mouse fibroblasts were cultured in medium containing 0.1% fetal bovine serum (FBS) for 6–7 days. The resulting G0 cells were reseeded in culture medium with or without 10 μM NU7026 containing 10% FBS 1.5 h prior to X-irradiation. Sixteen hours following X-ray irradiation, the culture medium was replaced with fresh medium and 5 days later, surviving colonies of cells were counted. These survival assays were performed in triplicate for each X-ray dose. 53BP1 deficient DT40 cells were previously described (24). Targeting constructs for chicken *Rad18* were designed as previously described (5). DT40 cells were cultured in RPMI1640 medium (Nissui) supplemented with 10% fetal calf serum (Valley Biomedical Inc.), 1% chicken serum (Medical and Biological Laboratories) and 10 μM β-mercaptoethanol at 39.5°C. X-irradiation at 150 kV and 20 mA was performed at a dose rate of 1.9 Gy/min with an X-ray irradiator (Hitachi Medico). The colony formation assay was performed as previously described (24). Briefly, an appropriate number of cells was plated

in 1.5% methylcellulose (Sigma)-containing medium immediately after irradiation. After incubation at 39.5°C for 7 days, the surviving cell fractions were calculated by comparing the numbers of colonies formed in the irradiated cultures with those in an unirradiated control.

For G1 phase synchronization, DT40 cells were treated with 1.0 μg/ml nocodazole (Sigma) for 8 h, washed three times with phosphate-buffered saline (PBS) containing 5% calf serum, and then cultured in medium containing 0.8 mM mimosine (Sigma) for 8 h. Synchronized cells were washed three times as described above and cultured in medium to release them into the cell cycle.

Plasmids, oligonucleotides and recombinant proteins

The bacterial expression vectors pGEX-3X-53BP1-N1, -N2, -N3, -N4, -CΔBRCT and -BRCT were previously described (19). Purification of the six GST fusion proteins encoded by the bacterial expression vectors was also previously described (19).

To obtain bacterially produced KBD-HA, we used PCR to generate a DNA fragment encoding amino-acid residues 1235–1616 of 53BP1 with a 3′ HA epitope tag. The product was inserted into the BamHI sites of pGEX6P-1. KBD-K1268R and -K1516R mutant were obtained by PCR using site-directed mutagenesis. The bacterially expressed GST-KBD-HA fusion protein was purified on Glutathione–Sepharose 4B resin (Amersham). If necessary, the GST moiety was subsequently removed from the fusion protein using PreScission Protease (Amersham). C-terminal myc-tagged wt or mutant RAD18 expression vectors were described elsewhere (6,41). Stealth siRNA specific for 53BP1 (5′-CUGAAAG CCAGGUUCUAGAGGAUGA-3′) and control Stealth siRNA (5′-CUGCGAGACUUGAUCGAGAGAAUG A-3′) were synthesized by Invitrogen Life Technologies. Stealth siRNAs specific for RAD6A, 6B (described for UBE2A, 2B, respectively) were purchased from Invitrogen Life Technologies. Cells were transfected with Stealth siRNA duplexes using Oligofectamine (Invitrogen) according to the manufacturer's instructions. To generate pEGFP-53BP1-C, pCMH6K53BP1 was digested with BamHI and XhoI and the 3′-fragment of 53BP1 was inserted into the BglII-SalI sites of pEGFP-C3 (Clontech). GFP-mouse53BP1-K1253R, pEGFP-53BP1-C-K1268R and pCMH6K53BP1-C-K1268R were obtained by PCR using site-directed mutagenesis. GFP-m53BP1 was a kind gift from Dr Y. Adachi.

In vitro ubiquitination assays

Wild-type and mutant RAD18–RAD6B complexes were purified from baculovirus-infected Sf9 cells (6) and then mixed with 100 ng E1, ubiquitin, GST-ubiquitin (Boston Biochem), and/or bacterially expressed KBD-HA in 30 μl reaction buffer (25 mM Tris–HCl, pH 7.6, 5 mM $MgCl_2$, 2 mM ATP, 0.5 mM dithiothreitol). After incubation for 30 min at 30°C, the reaction was stopped by the addition of SDS sample buffer, and the products were analyzed by western blotting with an anti-HA Ab.

Immunofluorescence analysis

Cells were washed twice with PBS, treated with 0.2% Nonidet P-40, and incubated on ice for 5 min. After incubation with NP-40, cells were pre-fixed with 3.7% formaldehyde in PBS for 5 min, washed again with PBS, and fixed with 80% methanol for 10 min at –20°C. Cells were stained with a specific primary Ab, then stained with species-specific Alexa Fluor 488 (Molecular Probes) or a rhodamine-conjugated secondary Ab (Cappel) and observed with a confocal laser-scanning microscope (FV300, Olympus).

In the case that cells containing RAD18 or 53BP1 foci per nucleus were scored, at least 100 cells per time point were analyzed for each experiment, and experiments were performed in triplicate.

Confluent MEF cells were used for γ-H2AX foci analysis. The cells were X irradiated (2 Gy) and then fixed after various lengths of time. The γ-H2AX foci were visualized by immunofluorescence staining, and the number of γ-H2AX foci per nucleus was counted. At least 40 cells per time point were analyzed for each experiment, and experiments were performed in triplicate.

Immunoprecipitation

Cells were homogenized in Buffer A (20 mM HEPES, pH 7.5, 10 mM KCl, 1 mM $MgCl_2$, 10% glycerol, 0.1% Nonidet P-40 and 1 mM phenyl methyl sulfonyl fluoride [PMSF)]) in a Dounce homogenizer on ice, and the nuclei were sedimented by centrifugation at 1000 rpm for 5 min. After the supernatant fraction was removed, the nuclear extracts were prepared by extraction with Buffer A containing 300 mM NaCl. For immunoprecipitation, nuclear extracts were mixed with an equal volume of Buffer A and pre-cleared with protein G-Sepharose (Amersham) for 30 min. The pre-cleared nuclear extracts were incubated with pre-immune serum, anti-53BP1 Ab (Oncogene), or anti-RAD18 Ab for 2 h, and then immunoprecipitated with protein G-Sepharose at 4°C. The precipitated products were analyzed by western blotting.

Pull-down assay

Recombinant GST-fused 53BP1 fragments bound to Glutathione–Sepharose 4B were incubated with HeLa cell lysates in lysis buffer (Buffer B; 50 mM Tris–HCl, pH 7.5, 150 mM NaCl, 0.2% Triton-X, 50 mM NaF, protease inhibitors). The beads were washed extensively with Buffer B, and bound proteins were analyzed by western blotting with an anti-RAD18 Ab. To examine the direct interaction between GST-RAD18 and KBD-HA *in vitro*, GST-RAD18 was overexpressed in Sf9 insect cells and purified using Glutathione–Sepharose 4B. Purified GST or GST-RAD18 was incubated with purified KBD-HA in buffer consisting of 50 mM HEPES, pH 7.5, 10 mM NaCl, 0.2% Triton X, 5% glycerol and 1 mM DTT at 4°C. Glutathione–Sepharose 4B was added to the reaction mixture, and the retrieved KBD-HA was analyzed by western blotting

using an anti-HA Ab. COS7 cells were transfected with RAD18-myc or RAD18C207F-myc and lysed in Buffer B. The lysates were incubated with recombinant GST-53BP1-N1 or GST-53BP1-CΔBRCT bound to Glutathione–Sepharose 4B. Precipitated proteins were analyzed by western blotting using an anti-myc Ab.

Isolation of the chromatin-enriched fractions

For immunostaining of salt-resistant IR-induced 53BP1 foci, cells were exposed to 5 Gy of X-ray, harvested 1 h later, and then treated with 40 μg/ml cycloheximide. One or three hours after addition of cycloheximide, cells were washed with cold PBS and then incubated on ice for 0.5 h in TNE buffer consisting of 50 mM Tris, pH 8.0, 300 mM NaCl, 1 mM EDTA, 0.2% Nonidet P-40, 1 mM PMSF, 1 μg/ml aprotinin, 10 μg/ml each pepstatin and leupeptin, and 50 mM NaF. After fixation of the cells, salt-resistant 53BP1 foci were visualized by immunofluorescence staining using an anti-53BP1 Ab (BP18), and nuclei were stained with 4′,6-diamidino-2-phenylindole (DAPI). At least 200 cells were scored, and the percentages of cells containing more than five 53BP1 foci were determined in three independent experiments.

Fluorescence recovery after photo-bleaching (FRAP)

FRAP experiments were performed using a Leica TCS DMIRE2 confocal laser-scanning microscope with a 63×/1.32 HCX PLAPO CS objective (Leica, Mannheim, Germany). Cells transfected with a plasmid expressing GFP-m53BP1 were cultured on 14 mm glass-bottom dishes (Matunami, Osaka, Japan) for 2 days. The transfected cells were treated with bleomycin (3 μg/ml) and incubated for 3 h before FRAP analysis. Before photobleaching, three images were captured with 15% laser power. GFP-m53BP1 fluorescence was then photobleached by two scans with a 488-nm argon laser at 100% power. For post-bleach recording, the fluorescence intensity within a region of interest was measured every 1.5 s at 15% laser power.

RESULTS

RAD18 forms nuclear foci at DSBs in response to IR

We previously showed that RAD18 relocalizes to form discrete nuclear foci, likely corresponding to sites of stalled replication, in response to a variety of genotoxic agents, including UV irradiation (8,12). We therefore compared the subcellular distribution of RAD18 in cells after UV- and IR- treatments. In response to UV-irradiation, RAD18 formed numerous nuclear foci (>80 per cell) that colocalized with PCNA (Figure 1A). In contrast, fewer foci (~50 per cell) were induced by X-ray irradiation. The X-ray-induced foci were larger than those induced by UV light and did not colocalize with PCNA (Figure 1A). This observation is consistent with our finding that PCNA is not monoubiquitinated in response to X-ray irradiation. Moreover, colocalization with PCNA was observed only in S-phase cells harboring stalled DNA replication forks, suggesting that the X-ray-induced RAD18 foci differ from those induced by UV light. Distinctive RAD18 nuclear foci were formed in mammalian cells exposed to X-rays, even in the presence of cycloheximide, indicating that focus formation does not require *de novo* protein synthesis (data not shown).

The histone variant H2AX is instantly phosphorylated at chromatin regions flanking DSBs, and the number of phosphorylated H2AX (γ-H2AX) foci in cells reflects the number of DSBs (17). To assess whether RAD18 forms nuclear foci at the chromatin flanking DSB sites, we examined the localization of RAD18 and γ-H2AX foci in cells exposed to IR. In the absence of X-ray exposure, RAD18 showed diffuse nuclear localization (Figure 1B, upper panel). After X-ray exposure, however, RAD18 formed nuclear foci that largely colocalized with γ-H2AX foci (Figure 1B, center panel). Exposure to bleomycin, another DSB-inducing agent, also caused RAD18 to form nuclear foci that colocalized with γ-H2AX foci (Figure 1B, lower panel). Taken together, these results indicate that RAD18 forms nuclear foci at DSBs.

In response to DSB formation, various proteins are recruited to the regions flanking the breaks to form IRIFs containing NBS1, phospho-ATM, BRCA1 and 53BP1 (13,14,18). To determine if RAD18 is recruited to IRIFs, we examined whether nuclear RAD18 foci colocalized with IRIF component proteins. In X-irradiated cells, RAD18 foci largely colocalized with IRIF component proteins including NBS1, pATM, BRCA1 and 53BP1 (Figure 1C). As shown in Figure 1D, RAD18 foci appeared within 15 min after X-ray exposure and reached a plateau at 30 min (~90% the cells contained RAD18 foci). Thirty minutes after irradiation, the number of cells containing RAD18 foci began to gradually decrease; after 24 h, the number of cells with nuclear RAD18 foci had returned to the background level (~10%) (Figure 1D). The kinetics with which RAD18 was recruited to nuclear foci following irradiation was similar to those for 53BP1 and γ-H2AX, known components of IRIF. These results indicate that RAD18 is a component of IRIFs.

X-ray-induced RAD18 focus formation is dependent on 53BP1 during G1 -phase

We next examined IR-induced RAD18 focus formation in various human cell lines defective for IRIF component proteins. Human cell lines deficient for NBS1, BRCA1 or ATM exhibited robust RAD18 focus formation in response to X-irradiation, indicating that the absence of these proteins does not affect this process (data not shown).

The similar kinetics with which RAD18 and 53BP1 foci formed following IR-treatment prompted us to examine whether 53BP1 is required for the IR-induced formation of RAD18 foci. To examine the role of 53BP1 in RAD18 focus formation, 53BP1 was depleted from MCF7 cells using a 53BP1-specific siRNA. More than 90% of the 53BP1 was depleted within 24 h of siRNA treatment, and the level of depletion was sustained for at least 72 h.

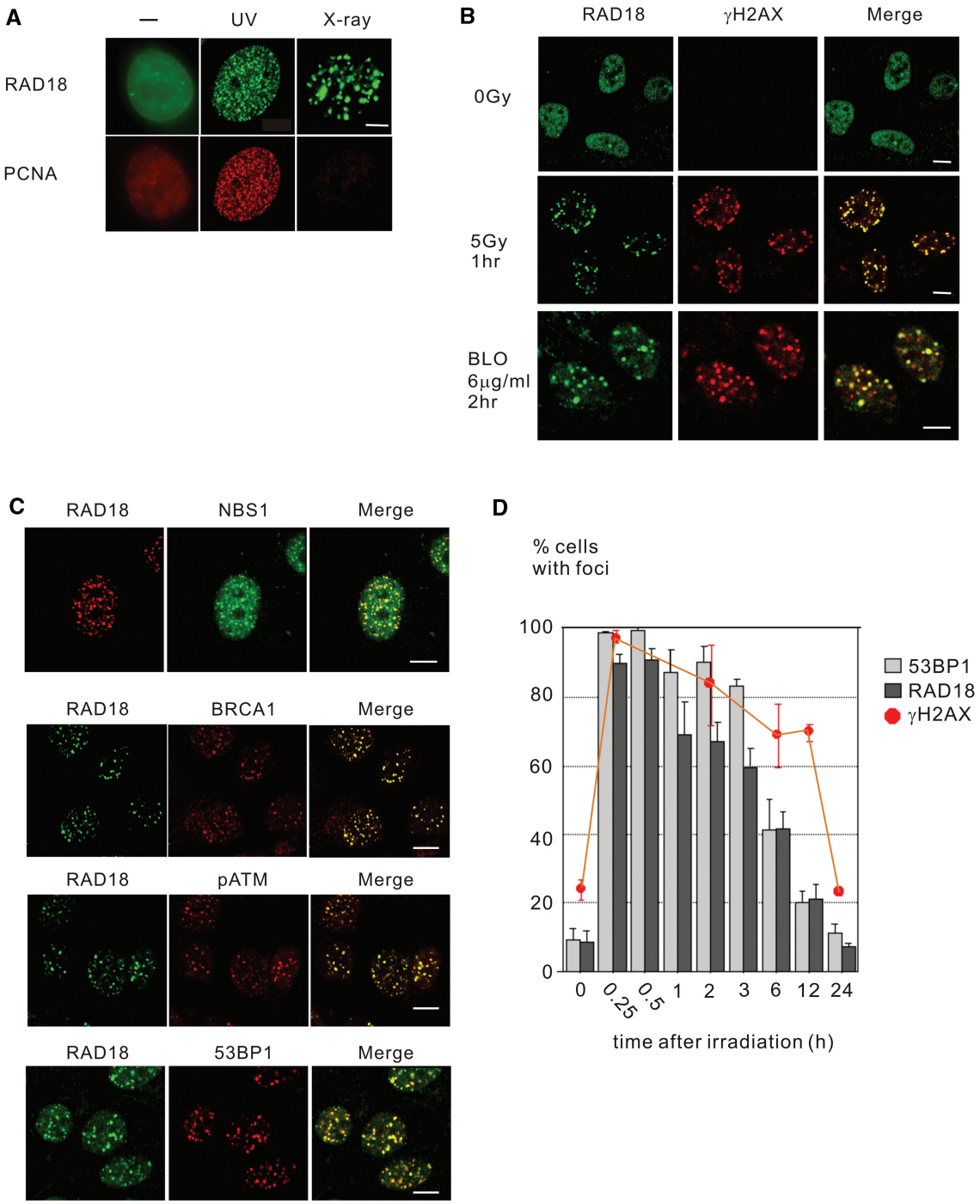

Figure 1. RAD18 foci colocalize with ionizing radiation-induced foci (IRIFs). (**A**) Human GM637 fibroblasts were non-irradiated or irradiated with UV light (10 J/m^2) or X-rays (5 Gy). The images shown are double-stained with anti-RAD18 and -PCNA antibodies (Abs). Bar = 5 μm (**B**) MCF7 cells were untreated, irradiated with X-rays, or treated with bleomycin (BLO). The images shown are double-stained with anti-RAD18 and γ-H2AX Abs. Bar = 5 μm (**C**) Human lung carcinoma H1299 (for NBS1 staining) or MCF7 cells were exposed to X-rays (5 Gy) and fixed 2 h later. The cells were then doubly immunostained with anti-NBS1, -BRCA1, -phospho-ATM, or -53BP1 Abs and anti-RAD18 Abs. Bar = 10 μm (**D**) Time course of RAD18 (dark grey), 53BP1 (light grey) or γ-H2AX (red) focus formation in MCF7 cells after X irradiation. MCF7 cells were exposed to X-rays (3 Gy) and allowed to recover for the lengths of time indicated. Cells containing more than five RAD18, 53BP1 or γ-H2AX foci per nucleus were scored.

The level of RAD18 was unaffected by 53BP1 depletion (Supplementary Figure 1). In the non-depleted cells, 53BP1 and RAD18 were homogeneously distributed throughout the nucleus prior to irradiation (Figure 2A). Following IR-treatment, RAD18 and 53BP1 formed discrete nuclear foci, however, in the 53BP1-depleted cells, the numbers of cells containing IR-induced RAD18 foci was reduced by ~35% relative to the controls

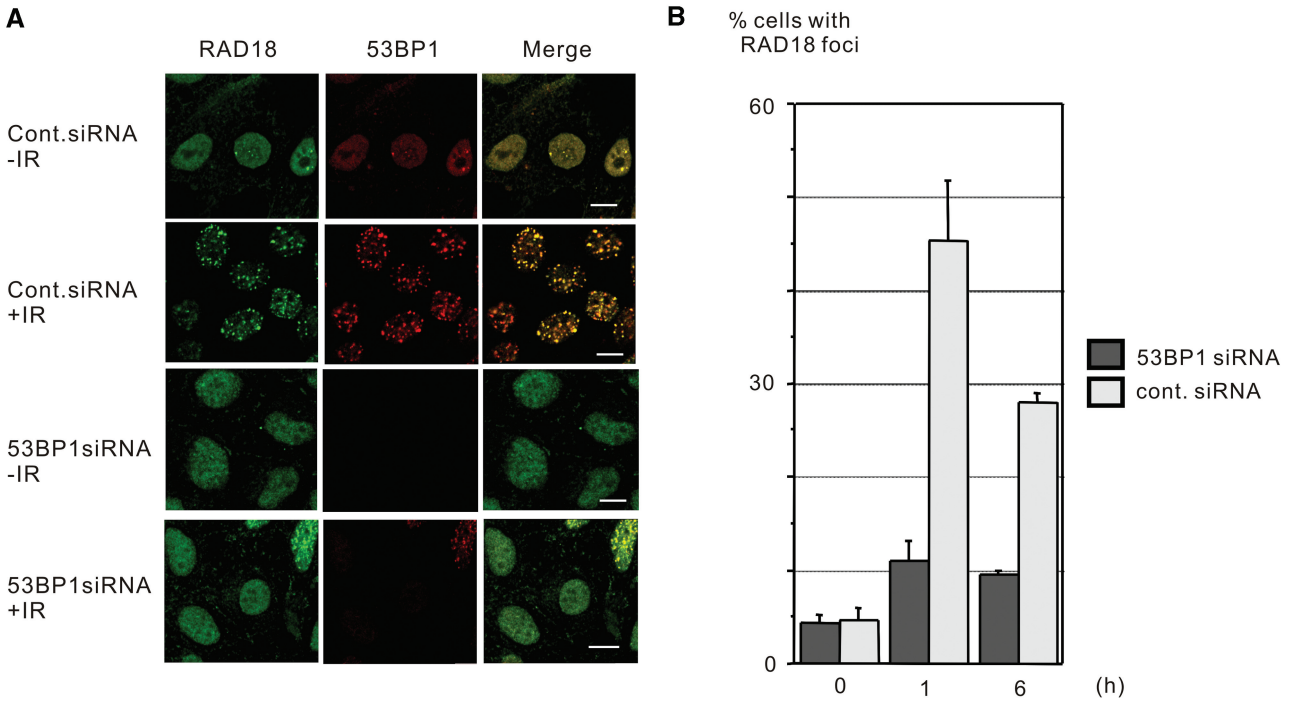

Figure 2. IR-induced RAD18 focus formation requires 53BP1. (**A**) MCF7 cells were treated with control or 53BP1-specific siRNA. After no treatment or X-ray irradiation (3 Gy), cells were doubly immunostained with anti-RAD18 and -53BP1 antibodies (Abs). Bar = 10 μm (**B**) The percentage of RAD18 foci-positive cells present (A) at the indicated intervals after IR is shown. At least 200 cells per time point were analyzed for each experiment, and experiments were performed in triplicate.

(Figure 2B). These results suggest that the formation of RAD18 nuclear foci at DSB sites is dependent on 53BP1. γ-H2AX and 53BP1 IRIF formation was observed in the wt and Rad18-null cells, indicating that RAD18 is not required for γ-H2AX or 53BP1 focus formation (data not shown).

Next, to examine whether RAD18 IRIF formation is dependent on the presence of 53BP1 or cell-cycle status, confluent wt and 53BP1-null mouse cells were synchronized at G1 and then irradiated with X-rays (Supplementary Figure 2A). RAD18-containing IRIF were observed in the wt cells but not in the 53BP1-null cells (Figure 3A, left). In contrast, RAD18 IRIFs were observed in the asynchronous cells irrespective of the presence of 53BP1 (Figure 3A, right). Next, we investigated whether RAD18 IRIFs are formed in 53BP1-depleted cells at S or G2/M phase. 53BP1-depleted HeLa cells synchronized at G1 also showed no IR-induced RAD18 focus formation, but the HeLa cells synchronized at S or G2/M showed RAD18 focus formation irrespective of the 53BP1 status (Figure 3B, Supplementary Figure 2B). Moreover, asynchronous 53BP1-null cells expressing GFP-RAD18 were immunostained with anti-PCNA and -p-histoneH3 antibodies (Abs) for the identification of cells at S and G2/M phase, respectively (Figure 3C). GFP-RAD18 IRIFs were observed in both the S- and G2/M-phase 53BP1-null cells. Taken together, these data indicate that RAD18 IRIF formation is dependent on 53BP1 and its dependency was restricted to G1-phase cells.

RAD18 directly associates with 53BP1 at DSBs

We hypothesized that RAD18 forms foci by interacting with 53BP1 after X-ray exposure. Therefore, we performed co-immunoprecipitation experiments to test potential associations of RAD18 and 53BP1 in irradiated (and unirradiated control) 293T cells. An interaction between RAD18 and 53BP1 was observed only in the X-ray-treated cells (Figure 4A, upper panel). The IR-dependent interaction between these two proteins was confirmed by reciprocal co-immunoprecipitation using anti-53BP1 Abs (Figure 4A, lower panel). Moreover, the interaction between these two proteins could be detected most efficiently in G1-phase (Supplementary Figure 3), consistent with our finding that 53BP1-dependent RAD18 IRIF are restricted to G1-phase (Figure 3).

To evaluate the biological significance of Rad18-53BP1 association, we first sought to determine the region of 53BP1 that is required for its interaction with RAD18. We expressed a series of recombinant fusion proteins consisting of 53BP1 fragments with N-terminal GST tags in bacteria and partially purified them using Glutathione beads (Figure 4B, upper panel). Interactions between the GST–53BP1 fusion proteins and RAD18 were assessed by a pull-down assay using HeLa whole-cell extracts. The fusion protein containing amino acids 1052–1709 of 53BP1 (GST–53BP1–CΔBRCT) retained the ability to retrieve RAD18 from the whole-cell extract, indicating that the BRCT domain of 53BP1 is not required for its interaction with RAD18 (Figure 4B, lower panel).

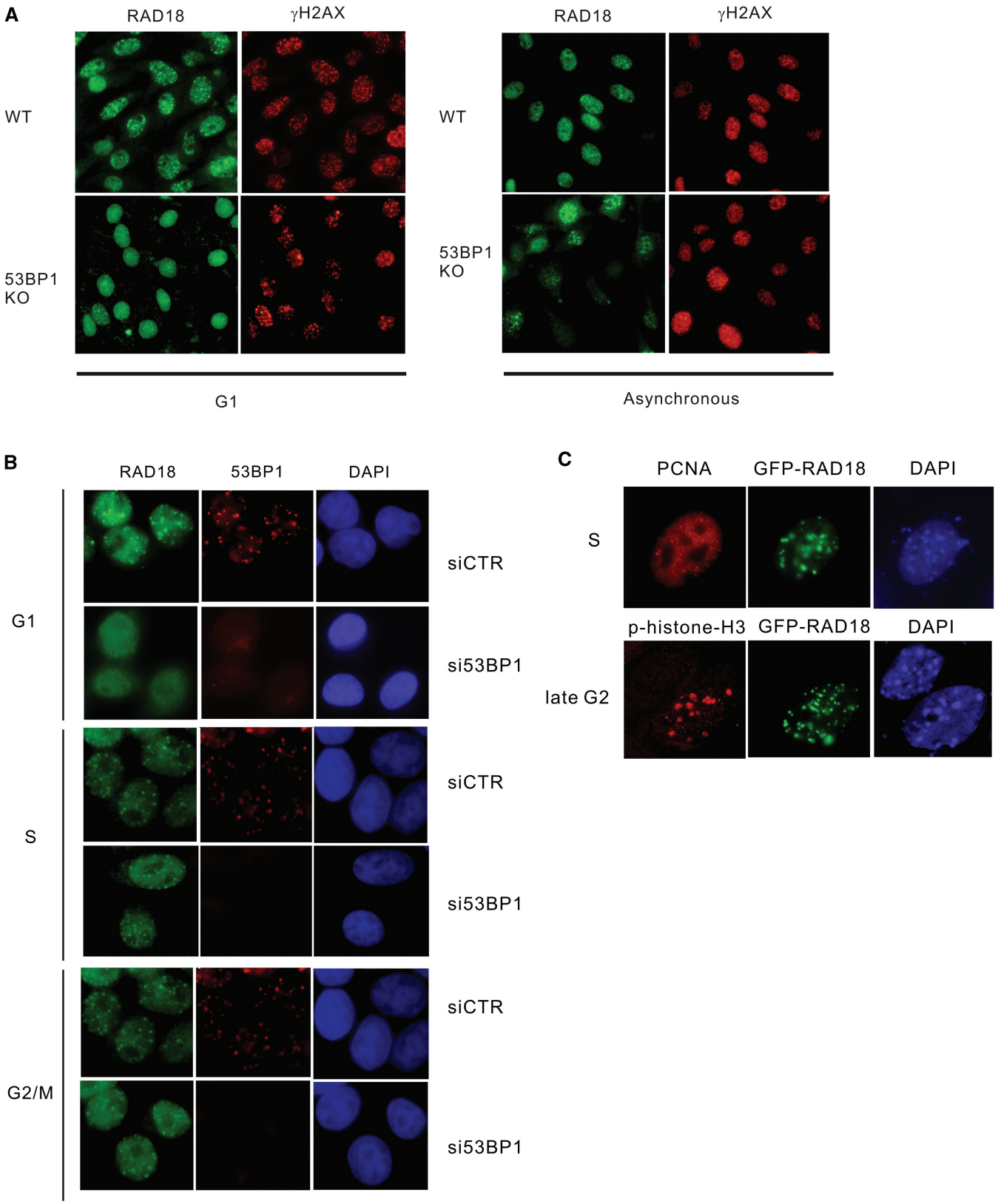

Figure 3. The 53BP1-dependent RAD18 IRIF formation is restricted to G1-phase. (**A**) G1-phase (left panel) or asynchronous (right panel) wt and 53BP1-null MEFs were irradiated with X-rays (5 Gy). Cells were harvested 1 h after irradiation and immunostained with the indicated Abs. (**B**) HeLa cells treated with control or 53BP1 siRNA were synchronized in S, G2/M and G1 phase by a double thymidine block. Then, the cells were exposed to X-rays (5 Gy) and fixed 1 h later. The cells were then doubly immunostained with anti-RAD18 and -53BP1 Abs. The synchronization efficiency of the cells was verified by FACS analysis. (**C**) The IRIF formation of GFP-RAD18 in 53BP1-null cells at S- and G2-phase. 53BP1-null MEFs were transfected with a GFP-RAD18 vector. Asynchronously growing cells were exposed to X-rays (5 Gy) and fixed 1 h later. GFP-RAD18 IRIFs were observed in the cells by immunostaining with anti-PCNA (S-phase) or -phospho-histone H3 (late G2-phase) antibodies (Abs).

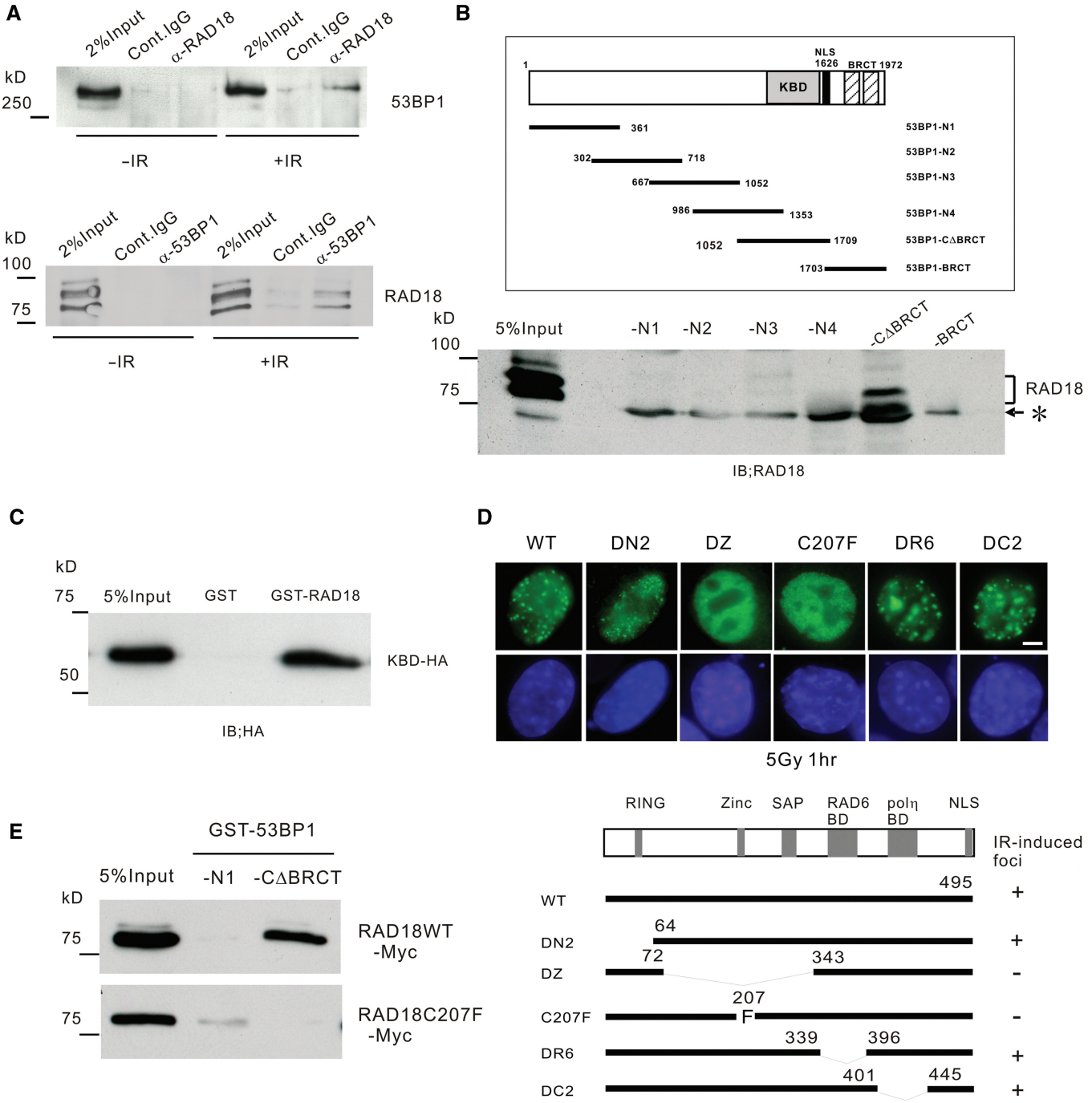

Figure 4. Association of RAD18 with 53BP1. (**A**) RAD18 binds 53BP1 in an IR-dependent manner. Nuclear extracts from X-irradiated (5 Gy) or untreated 293T cells were immunoprecipitated with anti-RAD18 antibodies (Abs) or control IgG. The precipitates were then analyzed by western blotting using anti-53BP1 Abs (upper panel). Alternatively, the nuclear extracts were immunoprecipitated with anti-53BP1 Abs and analyzed by western blotting using anti-RAD18 Abs. (lower panel) (**B**) GST-53BP1-CΔBRCT interacts with endogenous RAD18 in pull-down experiments. Schematic diagrams of N-terminal GST fusions of 53BP1 and its derivatives are shown. A series of GST-53BP1 fragments were bound to Glutathione–Sepharose and incubated with whole-cell extracts from unirradiated HeLa cells. Washed beads were analyzed by western blotting using anti-RAD18 Abs. An asterisk shows nonspecific bands. (**C**) The purified HA-tagged KBD fragment was incubated with GST-RAD18 or GST *in vitro*. Glutathione–Sepharose-bound proteins were analyzed by western blotting using anti-HA-tag Abs. (**D**) *Rad18*-null mouse cells were transiently transfected with myc-tagged wt or mutant RAD18, exposed to X-rays (5 Gy), and harvested 1 h later. Cells were then immunostained with anti-myc Abs, and the nuclei were stained with DAPI. Bar = 5 μm. Diagrams of myc-tagged wt, truncated and point mutants of RAD18 are shown. Locations of the RING, zinc-finger, SAP, RAD6-binding (RAD6BD), polη-binding (polηBD) domains and the nuclear localization signal (NLS) in RAD18 are indicated (lower panel). (**E**) COS7 cells were transfected with wt or zinc-finger mutant RAD18 tagged at the C-terminus with myc. Whole-cell lysates were then incubated with GST-53BP1-N1 or GST-53BP1-C-ΔBRCT (Figure 4B). The pulled-down proteins were analyzed by western blotting using anti-myc Abs.

Since the kinetochore-binding domain (KBD) of 53BP1 harbors a minimal region for focus formation after exposure to X-rays (19), we also assessed whether the KBD is required for the interaction of 53BP1 with RAD18. In an *in vitro* binding assay, the purified HA-tagged KBD fragment of 53BP1 bound purified GST–RAD18, but not the GST moiety alone (Figure 4C). These findings show that RAD18 interacts with 53BP1 via the KBD of 53BP1 and that the interaction between the two proteins is direct.

RAD18 interacts with 53BP1 *via* its zinc-finger domain, which is also required for RAD18 IRIF formation

Next, we sought to identify the region within RAD18 that is required for its recruitment to IRIFs and its interaction with 53BP1. To determine the region of RAD18 required for IRIF formation, we transfected *Rad18*-null cells with myc-tagged expression vectors encoding wt or mutant forms of RAD18. As shown in Figure 4D, localization to nuclear foci post-IR was observed for full-length RAD18 and several of the deletion mutants, but not for RAD18DZ, a mutant lacking the zinc-finger domain and its flanking regions, or C207F. These findings indicate that the zinc-finger domain of RAD18 is required for IRIF formation. Next, we tested whether RAD18 forms nuclear foci by using its zinc-finger domain to interact with 53BP1. C-terminal myc-tagged wt and C207F RAD18 were expressed in COS-7 cells and examined for their ability to interact with GST-53BP1-CΔBRCT in pull-down assays. As shown in Figure 4E, wt RAD18 was efficiently retrieved from COS-7 whole-cell extracts by GST-53BP1-CΔBRCT beads. In contrast, RAD18C207F was not recovered by GST-53BP1-CΔBRCT, indicating that 53BP1 interacts with RAD18 via the RAD18 zinc-finger domain.

A RAD18 complex monoubiquitinates, but does not poly-ubiquitinate, 53BP1 *in vitro*

Since our results showed that RAD18 directly associates with 53BP1 *in vitro* and in IR-treated cells, we considered the possibility that RAD18 monoubiquitinates or poly-ubiquitinates 53BP1. First, we examined whether purified RAD18–RAD6 complex could ubiquitinate 53BP1 *in vitro* using the purified HA-tagged KBD fragment of 53BP1 as a substrate. Ubiquitination of the 53BP1 KBD fragment was then analyzed by immunoblotting using anti-HA Abs (Figure 5A). In the presence of the RAD6–RAD18 complex, the KBD-HA fragment was detected as a more slowly migrating species than the unmodified HA-tagged KBD fragment. When ubiquitin was replaced with GST-ubiquitin in the assay, a much more slowly migrating band was detected. These results indicate that the RAD6–RAD18 complex monoubiquitinated the 53BP1 fragment. Notably, we did not detect poly-ubiquitination of the KBD fragment in this assay.

We next tested whether RAD18C207F, which does not interact with 53BP1, could also monoubiquitinate the KBD fragment. As shown in Figure 5B, RAD18C207F exhibited no ubiquitination activity towards the KBD fragment. In contrast with 53BP1, PCNA was efficiently monoubiquitinated by RAD18C207F *in vitro* (data not shown). Therefore, RAD18C207F retains ubiquitin ligase activity towards PCNA but not the 53BP1 KBD fragment. Most likely, the failure of RAD18C207F to ubiquitinate the KBD fragment is due to the inability of RAD18C207F and 53BP1 to interact. Therefore, we conclude that wt RAD18 functions as an E3 enzyme for the monoubiquitination of 53BP1 *in vitro*. Finally, to identify the site in 53BP1 that is monoubiquitinated by RAD18, we introduced point mutations into the putative monoubiquitination sites in KBD and used the purified fragments as substrates for *in vitro* ubiquitination assays with RAD18 (Figure 5C). The efficiency of monoubiquitination was remarkably reduced in the mutant K1268R. Taken together, we conclude that Lys 1268 of 53BP1 is specifically monoubiquitinated by RAD18 *in vitro*, although we could not detect monoubiquitinated form of endogenous 53BP1 *in vivo* (data not shown).

The retention of 53BP1 at DSBs is enhanced by the interaction of 53BP1 with RAD18 and by the function of RAD18–RAD6 complex

In the cellular response to IR, the exposure of methylated histones is required for the initial recruitment of 53BP1 to DSBs (20,21). Subsequently, the expansion of γ-H2AX surrounding the DNA breaks is promoted through protein-protein interactions and protein modification at the IRIF region, resulting in the retention of 53BP1 at the sites of breakage (22,23).

We hypothesized that the modification of 53BP1 itself by RAD18 may influence the proper localization of 53BP1 in response to IR, possibly contributing to its association with chromatin in the vicinity of DSBs. To assess this possibility, we determined the number of wt and *Rad18*-null mouse cells containing tightly-associated 53BP1 foci (which are resistant to salt-extraction) following X-ray irradiation.

To this end, cycloheximide was added to the cells 1 h after irradiation to block *de novo* protein synthesis. Irradiated cultures of wt and *Rad18*-null cells were incubated with cycloheximide for 1 or 3 h prior to extraction with a buffer containing 300 mM NaCl (to remove the loosely associated 53BP1 fraction from the chromatin).

In both wt and *Rad18*-null cells, >95% of the cells retained 53BP1 foci up to 1 h after the addition of cycloheximide (data not shown). In contrast, 3 h after the addition of cycloheximide, only 5% of the *Rad18*-null cells retained 53BP1 foci, compare to >30% in the wt cells (Figure 6A). 53BP1 retention was restored by the introduction of wt *Rad*18 but not by the expression of zinc-finger mutants of *Rad*18 (*Rad18*C207F) defective for both the interaction with 53BP1 and 53BP1-directed monoubiquitination. We also investigated the role of the E2 ligase RAD6, which cooperates with RAD18 to achieve the perform monoubiquitination and poly-ubiquitination of RAD18 substrates, in mediating the retention of 53BP1 foci after IR treatment. We generated a RAD18 deletion mutant lacking the RAD6-binding domain (*Rad18*DR6). Rad18DR6 was expected to display defective E3 ligase activity due to a failure to associate

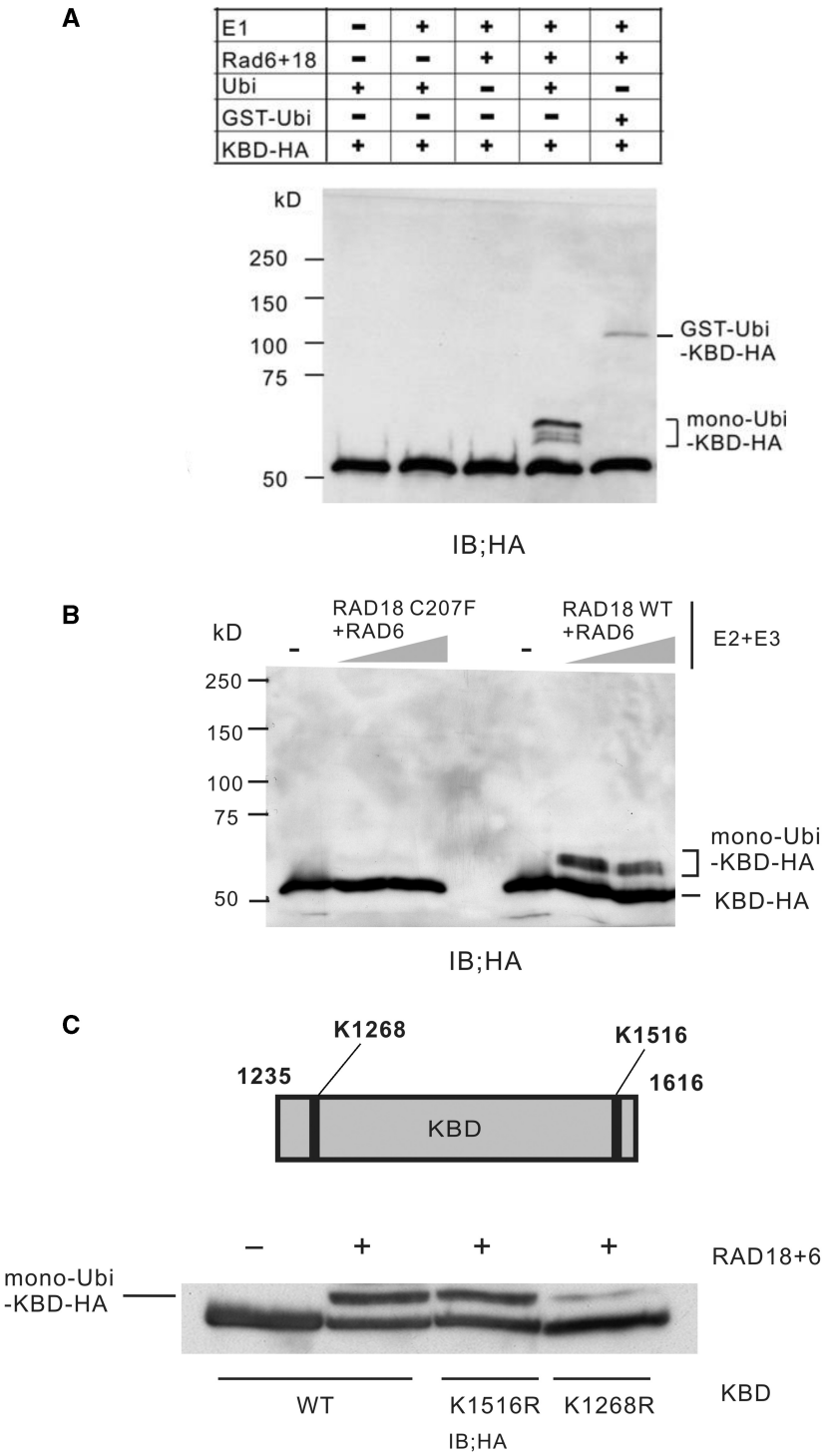

Figure 5. A RAD18–RAD6 complex mediates monoubiquitination of 53BP1 *in vitro* (**A**) Monoubiquitination of the 53BP1 KBD by RAD18 *in vitro*. A recombinant HA-tagged KBD fragment of 53BP1 was incubated with components of the ubiquitination system as indicated. The reactions were analyzed by western blotting using anti-HA antibodies (Abs). (**B**) The HA-tagged KBD fragment was incubated with wt or zinc-finger mutant RAD18 (C207F), together with other components of the ubiquitination system. The reactions were treated as in (A). (**C**) Recombinant WT or mutant KBD fragment, introduced point mutation into internal lysine residue (upper panel), were incubated with the RAD18–RAD6 complex in the ubiquitination system, as indicated. The reactions were treated as in (A).

with Rad6. As shown in Figure 6A, *Rad18*DR6 failed to correct the defective retention of 53BP1 foci at DSBs after IR treatment. To further confirm the requirement for the RAD18–RAD6 complex in mediating the retention of 53BP1 IRIFs, we used siRNA to ablate the expression of RAD6A and RAD6B. As shown in Figure 6B (right panel), we efficiently depleted RAD6A and RAD6B in U2OS cells.

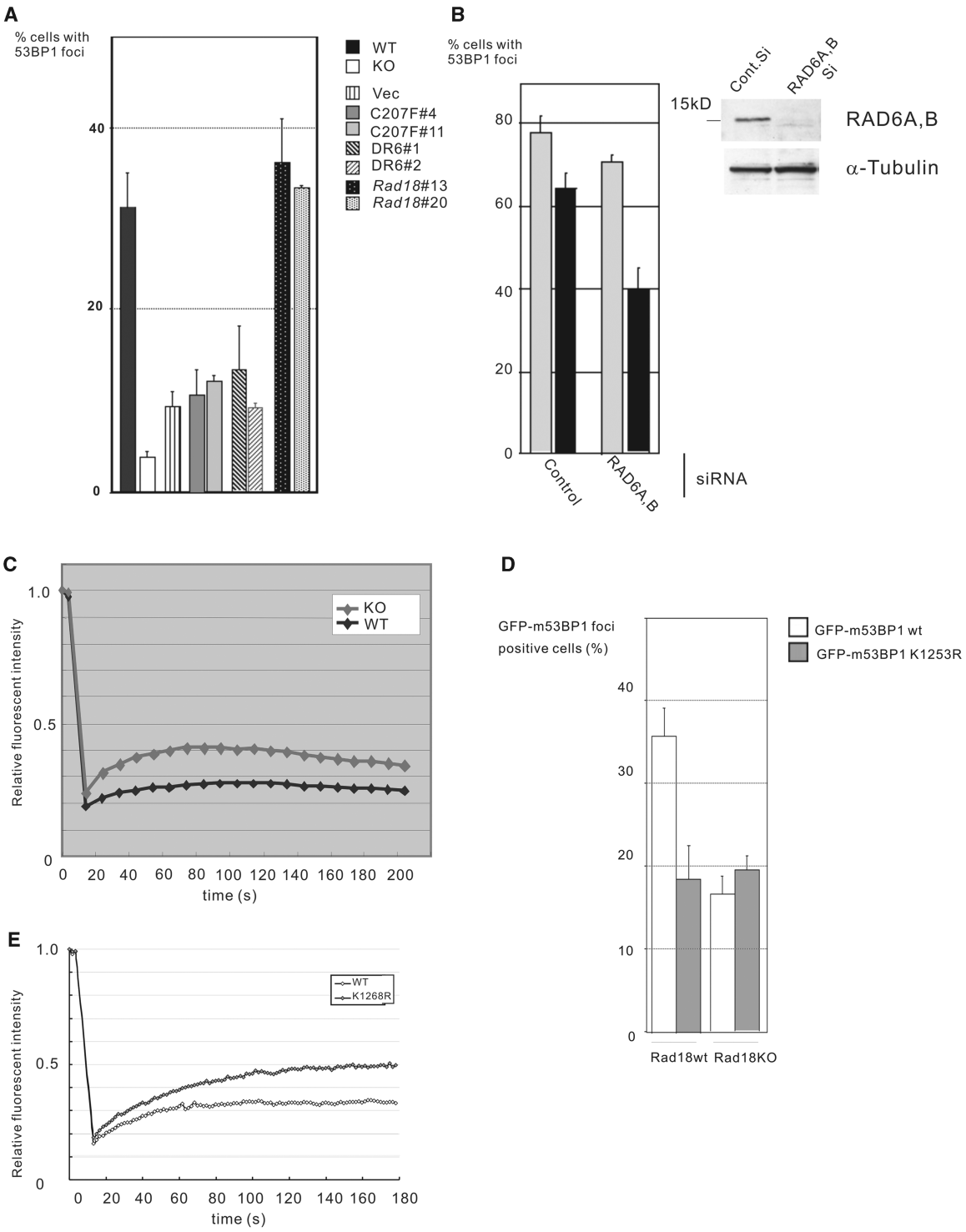

Figure 6. The stability of IR-induced 53BP1 foci is affected by RAD18. (**A**) *Rad18*-null (KO) or wt (shown as WT) mouse cells were exposed to X-rays (5 Gy) and harvested for 1 h. Following X-irradiation, Cycloheximide (40 μg/ml) was added, and salt-resistant 53BP1 foci were visualized by immunofluorescence staining 3 h later. The same experiments were also performed using *Rad18*-null mouse cells that stably expressed wt, zinc finger-mutant (C207F), Rad6-binding domain-defective *Rad18* (DR6) or a mock vector. The individual clone numbers are indicated. (**B**) U2OS cells were transfected with control or RAD6A,B-specific siRNA for 48h and analyzed by immunoblotting with anti-RAD6B antibodies (Abs). The cells were treated as in (A) (black bar) or were immunostained with anti-53BP1 Abs without pre-extraction with TNE buffer (gray bar). (**C**) Quantitative FRAP analysis of bleomycin-induced GFP-m53BP1 foci in *Rad18*-null (KO) or wt (WT) mouse cells. Each curve represents the average of three independent, normalized measurements. (**D**) The analysis of GFP-mouse 53BP1 (m53BP1) focus formation after bleomycin treatment. The full-length GFP-tagged m53BP1 WT or K1253R were transiently transfected into *Rad18* wt or *Rad18*-null mouse cells. After 24 h treated with 7 μg/ml bleomycin, GFP-m53BP1 foci positive cells were scored. At least 200 cells were analyzed for each experiment, and experiments were performed in triplicate. (**E**) U2OS cells stably expressing wt GFP-53BP1-C or mutated GFP-53BP1-C (K1268R) were treated with bleomycin. The recovery curve for bleomycin-induced GFP-53BP1-C foci in each of the cell lines were plotted.

We then compared the number of 53BP1 foci in control and RAD6A/6B siRNA-treated cells following X-ray irradiation. Without salt-extraction, similar numbers of the control and RAD6A/B-depleted cells contained 53BP1 foci. However, a reduced number of tightly associated salt-resistant 53BP1 foci were detected in the RAD6A/B-depleted cells relative to the cells transfected with a control siRNA (Figure 6B). These results raise the possibility that the interaction of 53BP1 with RAD18 and its subsequent RAD18–RAD6-mediated monoubiquitination promote the retention of 53BP1 at DSBs. To confirm that RAD18 stabilizes 53BP1 at chromatin regions near DSBs in living cells, we measured the dynamics of 53BP1 in bleomycin-induced foci using fluorescence-recovery after photobleaching (FRAP) technique. Mouse wt or *Rad18*-null cells were transiently transfected with GFP-mouse53BP1 (m53BP1) and then cultured in the presence of bleomycin. The FRAP analysis showed that in the wt cells, approximately 28% of the fluorescent signal was regained, whereas 42% of the signal was recovered in the *Rad18*-null cells (Figure 6C). Thus, the immobile fraction of GFP-m53BP1 at the DSBs was reduced in the *Rad18*-null cells (<60%), compared to the *Rad18* wt cells (>70%). Furthermore, we calculated the rate of the recovery by measuring the inclination of the curve obtained by the FRAP assay. *Rad18*-null cells showed about 1.9-fold higher inclination of the recovery curve of the GFP-m53BP1 than that of wt cells, suggesting the increase of dynamics of 53BP1 in the *Rad18*-null cells. These results support the idea that the association between GFP-m53BP1 and the DSB region is more stable in wt cells than in *Rad18*-null cells. In an attempt to test whether RAD18 affects the chromatin retention of 53BP1, we monitored bleomycin-induced GFP-m53BP1 foci in *Rad18*-null and wt cells (Figure 6D). In wt cells, the number of nuclei with bleomycin-induced foci of GFP-tagged mouse 53BP1 harboring the K1253R mutation, corresponding to human 53BP1 K1268R mutation, was reduced by 50% relative to that of wt GFP-m53BP1 24 h after treatment with bleomycin. In contrast, *Rad18*-null mouse cells showed almost no difference in the number of nuclei with bleomycin-induced foci between wt and mutant GFP-m53BP1. These results suggest that RAD18-directed modification at Lysine 1268 of 53BP1 promotes the retention of 53BP1 at DSBs. To further investigate whether RAD18-directed modification of 53BP1 affects retention of 53BP1 at DSBs, we used FRAP to compare the dynamics of GFP-fused wt C-terminal half of human 53BP1 fragment (amino-acid residues 1052–1972) with that mutated at K1268R. The mutated 53BP1 fragment at K1268R showed about 1.6-fold higher inclination of the recovery curve than that of wt 53BP1 fragment (Figure 6E). Therefore, the mutated 53BP1 fragment at K1268R protein exhibited more dynamic behavior in bleomycin-induced foci when compared with the wt GFP-53BP1. Our FRAP analyses support the idea that RAD18-directed modification promotes the retention of 53BP1 at DSBs.

RAD18 and 53BP1 constitute an epistatic DSB response pathway in G1 cells

53BP1 is involved in the end-joining repair of a subset of DNA DSBs. Chicken DT40 cells deficient in 53BP1 have increased sensitivity to IR in G1-early S phase, whereas HR plays only a modest role in DSB repair and cell survival (24). To gain insight into the function of Rad18 in the repair of IR-induced DNA damage, we examined the X-ray sensitivity of Rad18-deficient DT40 cells at various stages of the cell cycle. Cells were synchronized in G1 phase with mimosine after being released from nocodazole. Following their release from the mimosine-induced arrest, the synchronously progressing cells were X-irradiated at various time points and then seeded onto plates for colony survival assays. Flow cytometric analysis of the DNA content and bromodeoxyuridine (BrdU) uptake following the release from mimosine revealed that wt, 53BP1-deficient, and Rad18-deficient cells progressed similarly through the cell cycle (Supplementary Figure 4A). The wt cells showed a relatively stable level of sensitivity to IR throughout the cell cycle (Figure 7A, left panel). In contrast, similar to the 53BP1-deficient cells, the Rad18-deficient cells exhibited a higher level of sensitivity to irradiation during G1. The elevated X-ray sensitivity of the G1-synchronized Rad18-deficient cells was not evident when the cultures were irradiated during S phase or late S/G2 (2 h and 4 h after the release from mimosine, respectively). These data suggest that the repair of IR-induced DNA damage is impaired during G1 in Rad18-deficient cells. In parallel, we examined the UV sensitivity of DT40 cells deficient for 53BP1 or Rad18 at various stages of the cell cycle. 53BP1-deficient cells showed a slight increase in UV sensitivity during early S phase compared to wt DT40 cells (Figure 7A, right panel). In sharp contrast to the increased X-ray sensitivity observed during G1, the Rad18-deficient cells exhibited elevated UV sensitivity in early S phase, suggesting that there is distinct cell-cycle dependency on Rad18 in the response to DNA damage elicited by IR or UV.

To determine the relationship between Rad18 and 53BP1 in X-ray sensitivity, we performed epistasis analysis using cells irradiated during G1. Rad18- and 53BP1-deficient cells were more sensitive to X-rays than were wt cells, and the 53BP1-deficient cells were more sensitive than the Rad18-deficient cells. The X-ray sensitivity of cells deficient for both Rad18 and 53BP1 was similar to that of the 53BP1-deficient cells (Figure 7B, left panel). In contrast, as reported previously (24), cells deficient for both 53BP1 and Artemis were more sensitive than either of the single mutants (Figure 7B, right panel). Thus, Rad18 and 53BP1 are epistatic for cell survival, which suggests that Rad18 and 53BP1 function in the same pathway for the repair of IR-induced DNA damage. To confirm that the elevated X-ray sensitivity of the G1-synchronized Rad18-deficient cells is attributable to lack of Rad18-mediated modification of 53BP1, we reconstituted Rad18-deficient cells with wt or Rad18C214F, a chicken mutant Rad18 that corresponds to human Rad18C207F. The protein

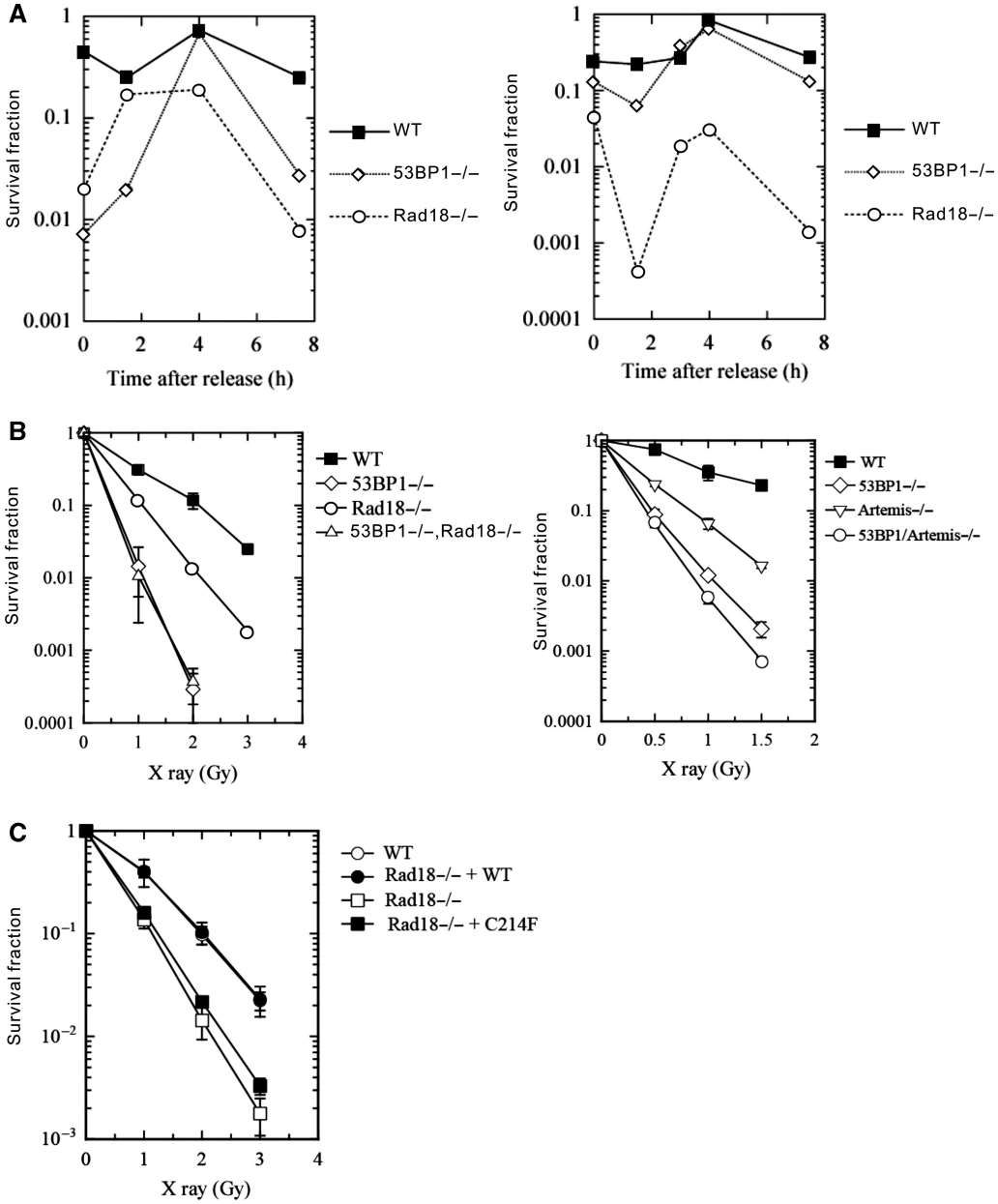

Figure 7. Divergent responses of 53BP1- and Rad18-deficient DT40 cells to X or UV irradiation. (**A**) Survival of wt, 53BP1-deficient and Rad18-deficient DT40 cells after X (left panel) or UV (right panel) irradiation. Cells synchronized in G1 phase were released into the cell cycle at time 0. The wt and 53BP1-deficient cells were treated with 1Gy of X-rays, while the Rad18-deficient cells were exposed to 2Gy of X-rays (left panel) or 5 J/m2 of UV (right panel) at the indicated time points then subjected to a colony formation assay. (**B**) Epistasis analysis between 53BP1 and Rad18 (left panel) or Artemis (right panel). 53BP1 and Rad18, but not Artemis, are epistatic in cell survival. G1-synchronized cells (Supplementary Figure 4B) were irradiated with the indicated dose of X-rays and subjected to a colony formation assay. Results represent the means ± SD from three independent experiments. (**C**) Complementation of Rad18-deficient cells by HA-tagged wt Rad18 (WT) or Rad18C214F (C214F). G1-synchronized cells were irradiated with the indicated dose of X-rays and subjected to a colony formation assay. Results represent the means ± SD from three independent experiments.

expression level of wt Rad18 and Rad18C214F was comparable (data not shown). Stable expression of wt Rad18, but not Rad18C214F, corrected the X-ray sensitivity of Rad18-deficient cells (Figure 7C), suggesting that modification of 53BP1 by RAD18 is important for Rad18-mediated repair of IR-induced DNA damage.

RAD18 and 53BP1 are involved in DSB repair during G1

To more closely examine the role of RAD18 in the DSB response pathway, we assessed DSB repair efficiency using the number of γ-H2AX foci as an index of the number of DSBs. The rate of loss of γ-H2AX foci is a direct marker of DSB repair in low-dose X-irradiated

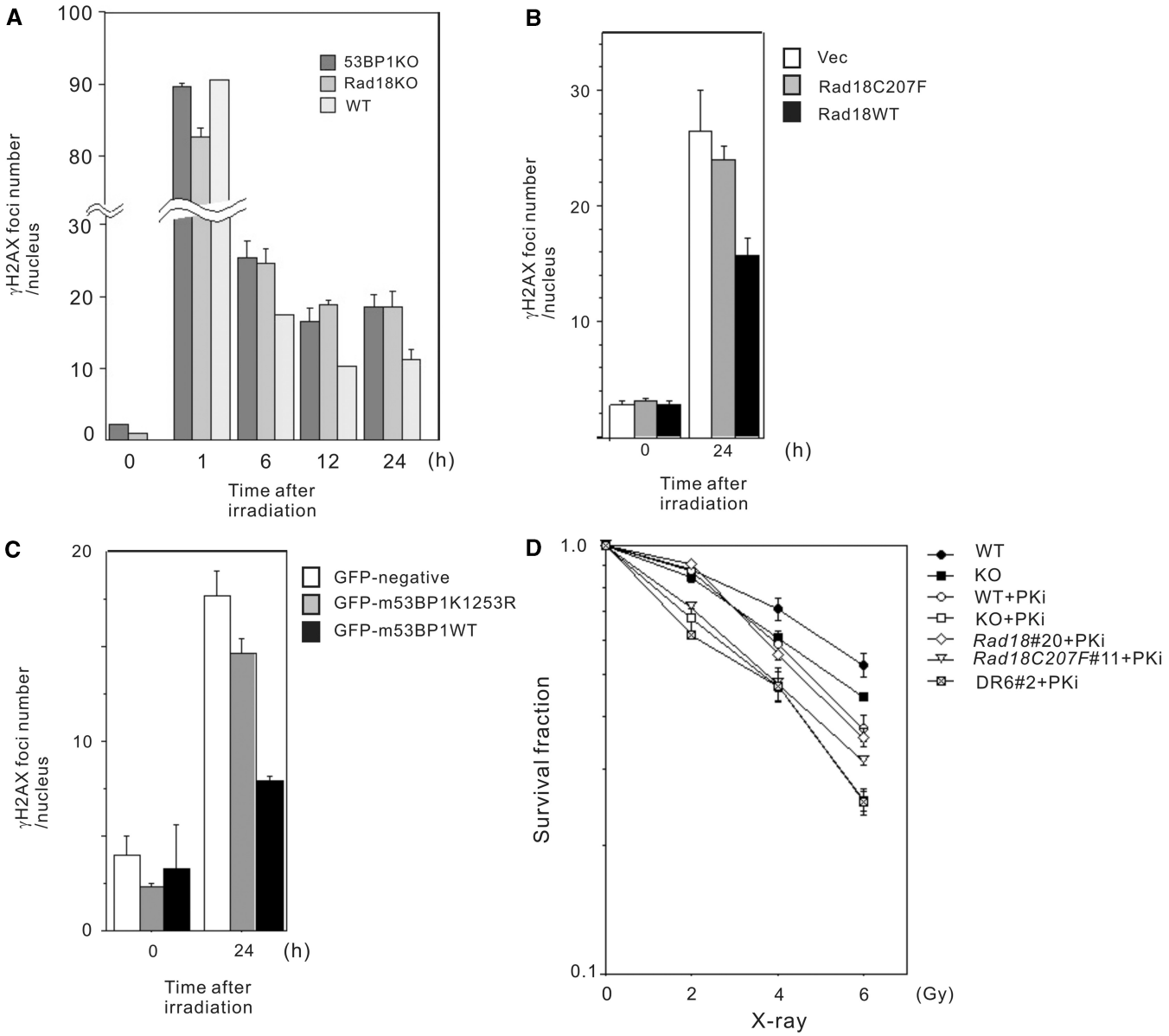

Figure 8. RAD18 is involved in the DSB repair during G1 phase. (**A**) Wild-type (WT) *Rad18*-null (Rad18KO) or *53BP1*-null (53BP1KO) MEFs were cultured until confluent and synchronized at G1 phase. Cells were irradiated with X-rays (2 Gy) in the presence of NU7026 and cultured for the indicated time. The cells were fixed and γ-H2AX foci were visualized by immunofluorescence staining. The number of γ-H2AX foci per nucleus was counted. (**B**) γ-H2AX foci analysis after γ-irradiation (2 Gy) in *Rad18*-null cells stably expressing wt Rad18, the zinc finger-mutant Rad18 (C207F) or a mock vector. The G1-enriched cells were treated with NU7026 for 1 h before X-irradiation. After 24 h, irradiated or non-irradiated cells (0 h) were fixed and γ-H2AX foci were visualized by immunofluorescence staining. The number of γ-H2AX foci per nucleus was counted. (**C**) The analysis of γ-H2AX after γ-irradiation (2 Gy) in *53BP1*-null MEFs transfected with GFP-mouse 53BP1(m53BP1) wt (WT) or K1253R vector. Confluent cells transfected with the indicated vectors were treated with NU7026 for 1 h before X-irradiation. After 24 h, irradiated or non-irradiated cells (0 h) were fixed and γ-H2AX foci were visualized by immunofluorescence staining. The number of γ-H2AX foci per nucleus of GFP-positive cells was counted. The number of γ-H2AX foci in GFP-negative cells was counted as a control. (**D**) Cologenic survival assay of G1-enriched mouse cells post-IR. Wt, *Rad18*-null or stable expressing clones (*Rad18*, *Rad18* C207F and *Rad18* DR6) were treated with or without DNA-PKcs inhibitor (PKi) prior to the indicated dose of IR.

cells (17). The 53BP1-mediated DSB repair mechanism is distinct from the repair pathway mediated by DNA-PKcs (24). To assess whether Rad18 is also involved in the pathway responsible for rejoining of DSB, we examined kinetics of formation of γ-H2AX foci formation in G1-synchronized mouse cells in the presence of the DNA-PKcs inhibitor NU7026. As shown in Figure 1D and Supplementary Figure 5, both DNA-PKcs inhibition and G1-synchronization did not affect the kinetics of Rad18 IRIF.

Confluent wt, *53BP1*- and *Rad18*-null MEFs, were synchronized at G1 then exposed to X-rays, and the numbers of γ-H2AX foci were quantified (Figure 8A, Supplementary Figure 2A). The numbers of γ-H2AX foci were similar in 53BP1- and Rad18-null MEFs at 1 h post-IR, suggesting that almost similar numbers of

DSBs were formed in these cells. Moreover, γ-H2AX foci disappeared with similar kinetics in *Rad18*-null and *53BP1*-null MEFs. At 12 h or 24 h post-IR, *Rad18*-null or the *53BP1*-null MEFs contained approximately twice as many γ-H2AX nuclear foci as wt MEFs. These results indicate that DSB repair is less efficient in *Rad18*-null MEFs than in wt MEFs when DNA-PKcs kinase activity is inhibited. We conclude that both Rad18 and 53BP1 contribute to DNA DSB repair during G1 independently of DNA-PK-mediated repair pathway.

To assess whether retention of 53BP1 at DSBs and putative monoubiquitination of 53BP1 plays a role in DSB repair during G1, the number of γ-H2AX foci at 24 h post-IR was counted in G1-enriched *Rad18*-null cells stably reconstituted with wt *Rad18* or *Rad18*C207F (Figure 8B). The disappearance of γ-H2AX foci at 24 h post-IR was restored by the expression of wt *Rad*18 but not by the expression of *Rad18*C207F. In similar experiments, the numbers of γ-H2AX foci remaining 24 h post-IR were determined in *53BP1*-null MEFs transiently reconstituted with GFP-tagged mouse wt or K1253R-mutated 53BP1. The disappearance of γ-H2AX foci at 24 h post-IR was restored by the expression of wt 53BP1 but not by the mutated 53BP1 at K1253R (Figure 8C). These results suggest that putative RAD18-directed modification of 53BP1 was required for DSB repair during G1.

Finally, to evaluate whether Rad18 is involved in DSB repair during G1 phase, we examined the IR-sensitivity of a G1-enriched population of mouse cells treated with the DNA-PKcs inhibitor NU7026. In the absence of the inhibitor, *Rad18*-null cells showed modest X-ray sensitivity compared to wt cells (Figure 8D). However, in the presence of the inhibitor, the *Rad18*-null cells showed significant sensitivity to X-rays compared to the wt cells. To confirm that the sensitivity of G1-phase *Rad18*-null cells to IR is attributable to *Rad18*-deficiency, we reconstituted *Rad18*-null cells with wt, *Rad18*C207F or *Rad18*DR6. As shown in Figure 8D, stable expression of wt Rad18, but not C207F or DR6, corrected the IR-sensitivity of *Rad18*-null cells. These results suggest that RAD18 is involved in one of the DNA DSB repair pathways.

DISCUSSION

RAD18 plays a pivotal role in post-replication DNA repair in human cells exposed to UV light. In response to UV irradiation, RAD18 forms nuclear foci, almost all of which colocalize with PCNA, suggesting that RAD18 is recruited to stalled replication forks (6). In the present study, cells exposed to X-rays formed distinct nuclear foci containing RAD18, which colocalized with γ-H2AX foci but not with PCNA (Figure 1A). These results suggest that in X-ray-irradiated cells, the recruitment of RAD18 to DSBs and its localization into foci occur in a replication-independent manner.

RAD18 is also involved in S-phase-specific single-strand break repair (10). It is recruited to single-strand break sites induced by UV-A laser irradiation (25). Although X-ray irradiation causes various types of DNA breaks, the IR-induced RAD18 foci that we observed likely represent DSBs based on their colocalization with γ-H2AX and other early markers of the response to DSBs (Figure 1B and C). In our study, the formation of RAD18 IRIFs in G1 cells was dependent on 53BP1 (Figure 3A and B). Given that RAD18 IRIFs were observed in S- and G2/M-phase cells irrespective of the presence of 53BP1, the mechanism responsible for the recruitment of RAD18 to DSBs in G1 cells differ from that in S- or G2/M-phase cells. Consistent with the G1-specific, and RAD18/53BP1-dependent mechanism for DSB repair, the physical interaction between these two proteins could be detected efficiently at G1-phase but not at S or G2/M-phase (Supplementary Figure 3). NHEJ is thought to work mainly during G1-phase and various proteins including 53BP1 are recruited to DSBs to perform DSBs repair. The G1-specific binding of RAD18 with 53BP1 and putative G1-specific chromatin structure might contribute to the G1-specific dependency on 53BP1 for RAD18 IRIF. The binding of full-length 53BP1 and RAD18 was observed only when cells were irradiated with IR (Figure 4A), whereas bacterially-expressed 53BP1 KBD domain specifically bound to purified RAD18 *in vitro* (Figure 4B and C). We speculate that the apparent discrepancy between *in vivo* and *in vitro* experiments arises because *in vivo* binding of full length of 53BP1 to RAD18 is usually strictly suppressed by other domains of 53BP1 or by 53BP1-binding proteins unless the suppression is released by IR-induced post-transcriptional modifications or changes in associations with binding partners.

To assess the role of RAD18 at different cell-cycle stages, we investigated the formation of nuclear foci by a Rad18 cysteine 207 (C207F) mutant. The C207F RAD18 mutant failed to form foci during G1-phase, S-phase or G2/M (data not shown). Because 53BP1 was dispensable for IRIF of RAD18 during S- or G2/M phase, molecules other than 53BP1 will likely interact with RAD18 following completion of G1. Previous studies have shown that the zinc finger is required for accumulation of hRAD18 at sites of DNA damage (25). Additionally, DNA-damage-induced poly-ubiquitin chains are produced on histone H2A and H2AX on damaged chromosomes after irradiation of X-ray. These poly-ubiquitin chains assemble additional DSB regulators (26,27). It was also reported that Rad18 binds poly-ubiquitin chains through its zinc finger domains (28). Moreover, Surface plasmon resonance analysis (using GST-fusions of wt or GST-C207F zinc fingers derived from hRAD18) revealed that the zinc finger is indeed important for binding to ubiquitin (29). Therefore, we conclude that the zinc finger domain of RAD18 interacts with multiple target(s), possibly including the poly-ubiquitin chains on histone H2A and H2AX, during different stages of the cell cycle.

In the early response to IR, local changes in chromatin structure are required for the initial recruitment of 53BP1 to DSBs. The initial recruitment of 53BP1 to DSBs was proposed to involve the indirect sensing of DSBs by 53BP1 through its interaction with the methylated

Lys 79 residue of histone H3 and Lys 20 of histone H4 in the higher-order chromatin structure (20,30). After 53BP1 is recruited, its retention at the chromatin surrounding the break requires MDC1. Histone H2AX phosphorylation mediated by ATM and MDC1, which is also required for the retention of 53BP1, is thought to be extended from the site of breakage (31). Therefore, the initial recruitment of 53BP1 to DSBs and the subsequent accumulation of 53BP1 at these sites are mechanically dissimilar processes. This study demonstrates that RAD18 monoubiquitinates fragments of 53BP1 *in vitro* and that RAD18–RAD6 complex plays a role in retaining 53BP1 near DSBs (Figure 6A and B). The extent of 53BP1 retention correlates well with its monoubiquitylation in cells expressing wt, C207F or DR6 mutant RAD18 (Figure 6A). Moreover, the introduction of K1268R mutation into human 53BP1 dramatically decreased the efficiency of monoubiquitylation of 53BP1 *in vitro* (Fig. 5C). Additionally, the introduction of K1253R mutation into mouse 53BP1 decreased the efficiency of its foci formation (Fig. 6D). These results suggest very strongly that 53BP1 monoubiquitylation and nuclear retention at DSBs are closely related.

A fragment of 53BP1 was efficiently monoubiquitinated by RAD18–RAD6 complex *in vitro*, however, monoubiquitination of endogenous 53BP1 could not be detected *in vivo*. After IR-irradiation, most of 53BP1 appear to be poly-ubiquitinated and degradated by the ubiquitin–proteasome system (32). Moreover, this ubiquitin–proteasome system is required for IR-induced 53BP1 foci formation at DSBs (33).

So the whole mechanism of 53BP1 foci formation remains to be elusive. We speculate that both mono- and poly-ubiquitinaiton of 53BP1 function cooperatively in the initial recuruitment and retention of 53BP1 IRIF at DSBs. Thus, we could not identify the monoubiquitination form of 53BP1 *in vivo*, distinguishing from poly-ubiquitinated form of 53BP1. Actually the poly-ubiquitination and degradation of 53BP1 were observed in Rad18-null cells as well as in wt cells (data not shown). Salt-resistant 53BP1 nuclear foci persisted for longer periods post-irradiation in wt cells than in *Rad18*-null cells. Consistent with this finding, our FRAP results showed that the association of 53BP1 with chromatin at DSBs was less stable in *Rad18*-null cells than in control cells. Moreover, the number of cells with IR-induced foci of GFP-53BP1 harboring K1268R (or K1253R in mouse 53BP1) mutation in wt cells decreased to the level in *Rad18*-null cells. (Figure 6D and E). Since IR-induced 53BP1 focus formation was observed even in *Rad18*-null cells, we infer that the initial recruitment of 53BP1 to chromatin is RAD18- independent whereas RAD18–RAD6-dependent modification of 53BP1 is important for the retention of 53BP1 at DSBs. However, we cannot entirely exclude the possibility that RAD18 ubiquitinates unidentified substrate(s), which indirectly influence the dynamics of 53BP1 at DSBs.

We attribute the decreased retention of the 53BP1 foci in *Rad18*-null mouse cells to the loss of an interaction between 53BP1 and RAD18 and to decreased modification of 53BP1. Even in wt mouse cells, the 53BP1 IRIFs gradually disappeared. The dissociation of 53BP1 from the foci has two possible causes. First, since γ-H2AX is required for the retention of 53BP1 at DSBs, γ-H2AX dephosphorylation by protein phosphatase 2A (34) may result in the dissociation of 53BP1 from DSBs. Second, since RAD18 foci appeared after IR exposure and disappeared with a time course almost identical to that of the 53BP1 foci (Figure 1D), the dissociation of RAD18 from 53BP1 may decrease the retention of both proteins at DSBs. The dissociation of RAD18 from 53BP1 may increase the accessibility of an unidentified protein to 53BP1, resulting in the dislocation of 53BP1 from DSBs. The modification of 53BP1 at lysine 1268 may promote interactions with the chromatin surrounding DSBs. Alternatively, since 53BP1 is a mediator of DSB signaling, the modification of 53BP1 at DSB sites may recruit putative adaptor protein(s) containing ubiquitin-binding domains to the DSBs. Appropriate localization of DNA repair proteins is crucial for their function. 53BP1 plays a role in a subset of DSB repair events (24,35,36). In this study, we demonstrated that 53BP1 IRIFs are stabilized at DSBs through the interaction of RAD18 with 53BP1 and through modification of 53BP1. In addition, putative modifications of RAD18, including monoubiqitination, phosphorylation or dephosphorylation may facilitate the interaction between RAD18 and 53BP1 in response to IR. We also found that a *Rad18*-null mutation caused inefficient DSB repair in MEFs even after 24 h of X-ray irradiation (Figure 8A). In addition, the *Rad18*-null cells were significantly more sensitive to X-rays than the wt cells under the DNA-PKcs-inactive condition. Therefore, we conclude that RAD18 is involved in a subset of DSB repair pathways by promoting stable retention of 53BP1 foci at DSBs. Since the defective DSB repair of *RAD18*-null cells was most evident in G1-synchronized cells (especially in the presence of a DNA-PKcs inhibitor) we speculate that RAD18 plays a role in DSB repair via the non-homologous end joining (NHEJ) pathway. This idea is supported by the fact that the recombinant KBD protein stimulates double-stranded DNA end-joining activity of DNA ligase IV/Xrcc4 complex *in vitro* (19), that 53BP1 mutants unable to accumulate at IRIFs cannot correct the DSB repair defect of 53BP1-null cells (36), and that 53BP1 is functionally involved in XRCC4-dependent NHEJ (37). Additionally, the most recent reports show that 53BP1 promotes NHEJ at telomere-breakage sites through tethering and/or increasing mobility of the DNA ends, and 53BP1 also promotes NHEJ for V(D)J recombination (38,39). Taken together, we assume that the 53BP1-directed NHEJ pathway is promoted by RAD18-directed modification of 53BP1 and/or interaction between RAD18 and 53BP1.

We performed additional assays to detect differences in levels of DSBs in Rad18-wt and -null cells by using pulse-field gel electrophoresis (PFGE). PFGE did not reveal differences between Rad18-wt and -null cells. It should be noted however that PFGE, Comet and related assays are inherently insensitive techniques which only detect large global changes in the integrity of genomic DNA. For example, 53BP1 is a bona-fide mediator of DSB signaling, yet other workers have shown that there is no

difference between the PFGE pattern of genomic DNA derived from 53BP1-wt and -null following X-ray irradiation (40). Therefore, it is most likely that differences in levels of DSBs between Rad18-wt and -null cells are below the sensitivity levels of conventional assays. Alternatively, it is possible that RAD18 and 53BP1-mediated mechanisms represent partially redundant or minor back-up pathways of DSB repair.

In summary, we identified 53BP1 as a substrate for RAD18 E3 monoubiquitination activity *in vitro*, and we demonstrated that modification of 53BP1 at lysine 1268 has a functional role in promoting the retention of 53BP1 at DSB sites and that RAD18 is involved in DSB repair. These results increase our understanding of the role of RAD18 in the cellular response to DSBs.

SUPPLEMENTARY DATA

Supplementary Data are available at NAR Online.

ACKNOWLEDGEMENTS

We thank Cyrus Vaziri and Tsuyoshi Ikura for critical reading of the manuscript and for their valuable comments and suggestions. We thank Dr Yasuhisa Adachi for the GFP-m53BP1 plasmid and Dr Junjie Chen for the 53BP1-null MEFs.

FUNDING

Grants-in-Aid for Scientific Research (18710047, 180139 and 18058017) from the Ministry of Education, Culture, Sports, Science and Technology of Japan. Funding for open access charge: Grants for Management (007-39100200) from the Ministry of Education, Culture, Sports, Science and Technology of Japan.

Conflict of interest statement. None declared.

REFERENCES

1. Bailly,V., Prakash,S. and Prakash,L. (1997) Domains required for dimerization of yeast Rad6 ubiquitin-conjugating enzyme and Rad18 DNA binding protein. *Mol. Cell Biol.*, **17**, 4536–4543.
2. Friedberg,E.C., Walker,G.C. and Siede,W. (1995) DNA damage tolerance and mutagenesis in eukaryotic cells. In *DNA Repair and Mutagenesis*. ASM Press, Washington, DC, pp. 523–593.
3. Tateishi,S., Sakuraba,Y., Masuyama,S., Inoue,H. and Yamaizumi,M. (2000) Dysfunction of human Rad18 results in defective postreplication repair and hypersensitivity to multiple mutagens. *Proc. Natl Acad. Sci. USA*, **97**, 7927–7932.
4. Tateishi,S., Niwa,H., Miyazaki,J., Fujimoto,S., Inoue,H. and Yamaizumi,M. (2003) Enhanced genomic instability and defective postreplication repair in RAD18 knockout mouse embryonic stem cells. *Mol. Cell Biol.*, **23**, 474–481.
5. Yamashita,YM., Okada,T., Matsusaka,T., Sonoda,E., Zhao,GY., Araki,K., Tateishi,S., Yamaizumi,M. and Takeda,S. (2002) RAD18 and RAD54 cooperatively contribute to maintenance of genomic stability in vertebrate cells. *EMBO J.*, **21**, 5558–5566.
6. Watanabe,K., Tateishi,S., Kawasuji,M., Tsurimoto,T., Inoue,H. and Yamaizumi,M. (2004) Rad18 guides polη to replication stalling sites through physical interaction and PCNA monoubiquitination. *EMBO J.*, **23**, 3886–3896.
7. Tsuji,Y., Watanabe,K., Araki,K., Shinohara,M., Yamagata,Y., Tsurimoto,T., Hanaoka,F., Yamamura,K., Yamaizumi,M. and Tateishi,S. (2008) Recognition of forked and single-stranded DNA structures by human RAD18 complexed with RAD6B protein triggers its recruitment to stalled replication forks. *Genes Cells*, **13**, 343–354.
8. Masuyama,S., Tateishi,S., Yomogida,K., Nishimune,Y., Suzuki,K., Sakuraba,Y., Inoue,H., Ogawa,M. and Yamaizumi,M. (2005) Regulated expression and dynamic changes in subnuclear localization of mammalian Rad18 under normal and genotoxic conditions. *Genes Cells*, **10**, 753–762.
9. Saberi,A., Hochegger,H., Szuts,D., Lan,L., Yasui,A., Sale,J.E., Taniguchi,Y., Murakawa,Y., Zeng,W., Yokomori,K. *et al.* (2007) RAD18 and poly(ADP-ribose) polymerase independently suppress the access of nonhomologous end joining to double-strand breaks and facilitate homologous recombination-mediated repair. *Mol. Cell Biol.*, **27**, 2562–2571.
10. Shiomi,N., Mori,M., Tsuji,H., Imai,T., Inoue,H., Tateishi,S., Yamaizumi,M. and Shiomi,T. (2007) Human RAD18 is involved in S phase-specific single-strand break repair without PCNA monoubiquitination. *Nucleic Acids Res.*, **35**, e9.
11. Kannouche,PL., Wing,J. and Lehmann,A.R. (2004) Interaction of human DNA polymerase eta with monoubiquitinated PCNA: a possible mechanism for the polymerase switch in response to DNA damage. *Mol. Cell*, **14**, 491–500.
12. Bi,X., Barkley,LR., Slater,DM., Tateishi,S., Yamaizumi,M., Ohmori,H. and Vaziri,C. (2006) Rad18 regulates DNA polymerase kappa and is required for recovery from S-phase checkpoint-mediated arrest. *Mol. Cell Biol.*, **26**, 3527–3540.
13. Paull,T.T., Rogakou,E.P., Yamazaki,V., Kirchgessner,C.U., Gellert,M. and Bonner,W.M. (2000) A critical role for histone H2AX in recruitment of repair factors to nuclear foci after DNA damage. *Curr. Biol.*, **10**, 886–895.
14. Schultz,L.B., Chehab,N.H., Malikzay,A. and Halazonetis,T.D. (2000) p53 binding protein 1 (53BP1) is an early participant in the cellular response to DNA double-strand breaks. *J. Cell Biol.*, **151**, 1381–1390.
15. Celeste,A., Petersen,S., Romanienko,P.J., Fernandez-Capetillo,O., Chen,H.T., Sedelnikova,OA., Reina-San-Martin,B., Coppola,V., Meffre,E., Difilippantonio,M.J. *et al.* (2002) Genomic instability in mice lacking histone H2AX. *Science*, **296**, 922–927.
16. Stucki,M. and Jackson,S.P. (2006) gammaH2AX and MDC1: anchoring the DNA-damage-response machinery to broken chromosomes. *DNA Repair*, **5**, 534–543.
17. Rothkamm,K. and Lobrich,M. (2003) Evidence for a lack of DNA double-strand break repair in human cells exposed to very low x-ray doses. *Proc. Natl Acad. Sci. USA*, **100**, 5057–5062.
18. Bakkenist,CJ. and Kastan,M.B. (2003) DNA damage activates ATM through intermolecular autophosphorylation and dimer dissociation. *Nature*, **421**, 499–506.
19. Iwabuchi,K., Basu,B.P., Kysela,B., Kurihara,T., Shibata,M., Guan,D., Cao,Y., Hamada,T., Imamura,K., Jeggo,P.A. *et al.* (2003) Potential role for 53BP1 in DNA end-joining repair through direct interaction with DNA. *J. Biol. Chem.*, **278**, 36487–36495.
20. Huyen,Y., Zgheib,O., Ditullio,RA. Jr., Gorgoulis,VG., Zacharatos,P., Petty,T.J., Sheston,E.A., Mellert,H.S., Stavridi,E.S. and Halazonetis,T.D. (2004) Methylated lysine 79 of histone H3 targets 53BP1 to DNA double-strand breaks. *Nature*, **432**, 406–411.
21. Sanders,S.L., Portoso,M., Mata,J., Bahler,J., Allshire,R.C. and Kouzarides,T. (2004) Methylation of histone H4 lysine 20 controls recruitment of Crb2 to sites of DNA damage. *Cell*, **119**, 603–614.
22. Bekker-Jensen,S., Lukas,C., Melander,F., Bartek,J. and Lukas,J. (2005) Dynamic assembly and sustained retention of 53BP1 at the sites of DNA damage are controlled by Mdc1/NFBD1. *J. Cell Biol.*, **170**, 201–211.
23. Lou,Z., Minter-Dykhouse,K., Franco,S., Gostissa,M., Rivera,M.A., Celeste,A., Manis,J.P., van Deursen,J., Nussenzweig,A., Paull,T.T. *et al.* (2006) MDC1 maintains genomic stability by participating in the amplification of ATM-dependent DNA damage signals. *Mol. Cell*, **21**, 187–200.
24. Iwabuchi,K., Hashimoto,M., Matsui,T., Kurihara,T., Shimizu,H., Adachi,N., Ishiai,M., Yamamoto,K., Tauchi,H., Takata,M. *et al.* (2006) 53BP1 contributes to survival of cells irradiated with X-ray during G1 without Ku70 or Artemis. *Genes Cells*, **11**, 935–948.

25. Nakajima,S., Lan,L., Kanno,S., Usami,N., Kobayashi,K., Mori,M., Shiomi,T. and Yasui,A. (2006) Replication-dependent and -independent responses of RAD18 to DNA damage in human cells. *J. Biol. Chem.*, **281**, 34687–34695.
26. Huen,M.S., Grant,R., Manke,I., Minn,K., Yu,X., Yaffe,M.B. and Chen,J. (2007) RNF8 transduces the DNA-damage signal via histone ubiquitylation and checkpoint protein assembly. *Cell*, **131**, 901–914.
27. Mailand,N., Bekker-Jensen,S., Faustrup,H., Melander,F., Bartek,J., Lukas,C. and Lukas,J. (2007) RNF8 ubiquitylates histones at DNA double-strand breaks and promotes assembly of repair proteins. *Cell*, **131**, 887–900.
28. Bish,R.A. and Myers,M.P. (2007) Werner helicase-interacting protein 1 binds polyubiquitin via its zinc finger domain. *J. Biol. Chem.*, **282**, 23184–23193.
29. Notenboom,V., Hibbert,R.G., van Rossum-Fikkert,S.E., Olsen,J.V., Mann,M. and Sixma,T.K. (2007) Functional characterization of Rad18 domains for Rad6, ubiquitin, DNA binding and PCNA modification. *Nucleic Acids Res.*, **35**, 5819–5830.
30. Botuyan,M.V., Lee,J., Ward,I.M., Kim,J.E., Thompson,J.R., Chen,J. and Mer,G. (2006) Structural basis for the methylation state-specific recognition of histone H4-K20 by 53BP1 and Crb2 in DNA repair. *Cell*, **127**, 1361–1373.
31. Stucki,M., Clapperton,J.A., Mohammad,D., Yaffe,M.B., Smerdon,S.J. and Jackson,S.P. (2005) MDC1 directly binds phosphorylated histone H2AX to regulate cellular responses to DNA double-strand breaks. *Cell*, **123**, 1213–1226.
32. Zhang,D., Zaugg,K., Mak,T.W. and Elledge,S.J. (2006) A role for the deubiquitinating enzyme USP28 in control of the DNA-damage response. *Cell*, **126**, 529–542.
33. Jacquemont,C. and Taniguchi,T. (2007) Proteasome function is required for DNA damage response and fanconi anemia pathway activation. *Cancer Res.*, **67**, 7395–7405.
34. Chowdhury,D., Keogh,M.C., Ishii,H., Peterson,C.L., Buratowski,S. and Lieberman,J. (2005) gamma-H2AX dephosphorylation by protein phosphatase 2A facilitates DNA double-strand break repair. *Mol. Cell*, **20**, 801–809.
35. Riballo,E., Kuhne,M., Rief,N., Doherty,A., Smith,G.C., Recio,M.J., Reis,C., Dahm,K., Fricke,A., Krempler,A. *et al.* (2004) A pathway of double-strand break rejoining dependent upon ATM, Artemis, and proteins locating to gamma-H2AX foci. *Mol. Cell*, **16**, 715–724.
36. Ward,I., Kim,J.E., Minn,K., Chini,C.C., Mer,G. and Chen,J. (2006) The tandem BRCT domain of 53BP1 is not required for its repair function. *J. Biol. Chem.*, **281**, 38472–38477.
37. Xie,A., Hartlerode,A., Stucki,M., Odate,S., Puget,N., Kwok,A., Nagaraju,G., Yan,C., Alt,F.W., Chen,J. *et al.* (2007) Distinct roles of chromatin-associated proteins MDC1 and 53BP1 in mammalian double-strand break repair. *Mol. Cell*, **28**, 1045–1057.
38. Dimitrova,N., Chen,Y.C., Spector,D.L. and de Lange,T. (2008) 53BP1 promotes non-homologous end joining of telomeres by increasing chromatin mobility. *Nature*, **456**, 524–528.
39. Difilippantonio,S., Gapud,E., Wong,N., Huang,C.Y., Mahowald,G., Chen,H.T., Kruhlak,M.J., Callen,E., Livak,F., Nussenzweig,M.C. *et al.* (2008) 53BP1 facilitates long-range DNA end-joining during V(D)J recombination. *Nature*, **456**, 529–533.
40. Ward,I.M., Reina-San-Martin,B., Olaru,A., Minn,K., Tamada,K., Lau,J.S., Cascalho,M., Chen,L., Nussenzweig,A., Livak,F. *et al.* (2004) 53BP1 is required for class switch recombination. *J. Cell Biol.*, **165**, 459–464.
41. Miyase,S., Tateishi,S., Watanabe,K., Tomita,K., Suzuki,K., Inoue,H. and Yamaizumi,M. (2005) Differential regulation of Rad18 through Rad6-dependent mono- and poly-ubiquitination. *J. Biol. Chem.*, **280**, 515–524.